Technical Note: A Novel Geometric Morphometric Approach to the Study of Long Bone Shape Variation

Mélanie A. Frelat,[1,2]* Stanislav Katina,[3,4,5] Gerhard W. Weber,[6] and Fred L. Bookstein[6,7]

[1]*Dipartimento di Storie e Metodi per la Conservazione dei Beni Culturali, University of Bologna, 48121 Ravenna, Italy*
[2]*UMR 7268, University of Aix-Marseille – EFS - CNRS, 13334 Marseille, France*
[3]*Department of Anthropology, Faculty of Science, Masaryk University, Kotlářská 2, 611 37 Brno, Czech Republic*
[4]*Department of Mathematics and Statistics, Faculty of Science, Masaryk University, Kotlářská 2, 611 37 Brno, Czech Republic*
[5]*School of Mathematics and Statistics, University of Glasgow, Glasgow G12 8QW, UK*
[6]*Department of Anthropology, University of Vienna, Althanstrasse 14, 1090 Vienna, Austria*
[7]*Department of Statistics, University of Washington, Seattle, WA 98195-4322*

KEY WORDS tibia; hominoids; semilandmarks; artificial affine transformation; locomotion

ABSTRACT Procrustes-based geometric morphometrics (GM) is most often applied to problems of craniofacial shape variation. Here, we demonstrate a novel application of GM to the analysis of whole postcranial elements in a study of 77 hominoid tibiae. We focus on two novel methodological improvements to standard GM approaches: 1) landmark configurations of tibiae including 15 epiphyseal landmarks and 483 semilandmarks along articular surfaces and muscle insertions along the tibial shaft and 2) an artificial affine transformation that sets moments along the shaft equal to the sum of the moments estimated in the other two anatomical directions. Diagrams of the principal components of tibial shapes support most differences between human and non-human primates reported previously. The artificial affine transformation proposed here results in an improved clustering of the great apes that may prove useful in future discriminant or clustering studies. Since the shape variations observed may be related to different locomotor behaviors, posture, or activity patterns, we suggest that this method be used in functional analyses of tibiae or other long bones in modern populations or fossil specimens. Am J Phys Anthropol 149:628–638, 2012.

Geometric morphometrics (GM) allows researchers to quantify the geometry of complex biological forms and to compare them using statistics that consider the average form as well as the variation around it. While GM has been typically applied in this sense to cranial and mandibular morphology (e.g., Bookstein et al., 1999; Vidarsdottir et al., 2002; Harvati, 2003; Bastir and Rosas, 2006; Weber et al., 2006; Coquerelle et al., 2011), applications to the postcranial skeletal elements are uncommon (e.g., O'Higgins, 2000, Bouhallier et al., 2004; Taylor and Slice, 2005). Most of the analyses of the lower limb (e.g., Harmon, 2006, 2009a,b; Jungers et al., 2009; De Groote, 2011) have been limited to certain anatomical areas such as epiphyseal morphology, owing to the absence of appropriate landmarks on long bone diaphyses. Apart from an automatic feature detection algorithm developed to analyze sex differences in femur size and shape (Mahfouz et al., 2007), there seem to be no quantitative statements about the geometry of entire long bones using landmark identification. Nevertheless, the method of sliding semilandmarks (Bookstein, 1997; Gunz et al., 2005) allows the description of curves such as crests or ridges along the bone shaft by geometrically homologous points. The homology of those semilandmarks comes from the structures from which they are derived (e.g., attachments of muscles, articular surfaces). Because semilandmarks slide on curves derived from biologically homologous structures, their position on the curve itself remains a geometrical homology.

Tibial morphology includes information about phylogenetic history, mode of locomotion, and substrate preference because the tibia is the element transmitting body weight from the condyles of the femur to the foot (Lewis, 1989; Ruff, 2002). Differences between human and ape tibiae are often described qualitatively (Fig. 1a) or with simple measurements (e.g., Stern and Susman, 1983; Tardieu, 1981; Senut and Tardieu, 1985; Jungers, 1987; Stern, 2000; Marchi, 2007). Those differences are mainly attributed to different locomotor modes: bipedalism, arboreal or terrestrial quadrupedalism, and suspensory behavior. Most of those morphological features are often used for the assessment of fossil specimens as well (e.g., Trinkaus, 1975; Tardieu, 1988; Latimer et al., 1987; Berger and Tobias, 1995; Stringer et al., 1998; Lovejoy et al., 2009; Zipfel et al., 2011).

Grant sponsor: EU PF6 Marie Curie Actions grant (EVAN, Human Resource and Mobility Activity); Grant number: MRTN-CT-2005-019564.

*Correspondence to: Mélanie A. Frelat, Dipartimento di Storie e Metodi per la Conservazione dei Beni Culturali, Università di Bologna, Via degli Ariani, 1, 48121 Ravenna (RA), Italy.
E-mail: melanieagnes.frelat@unibo.it

Received 1 February 2012; accepted 19 September 2012

DOI 10.1002/ajpa.22177
Published online 2 November 2012 in Wiley Online Library (wileyonlinelibrary.com).

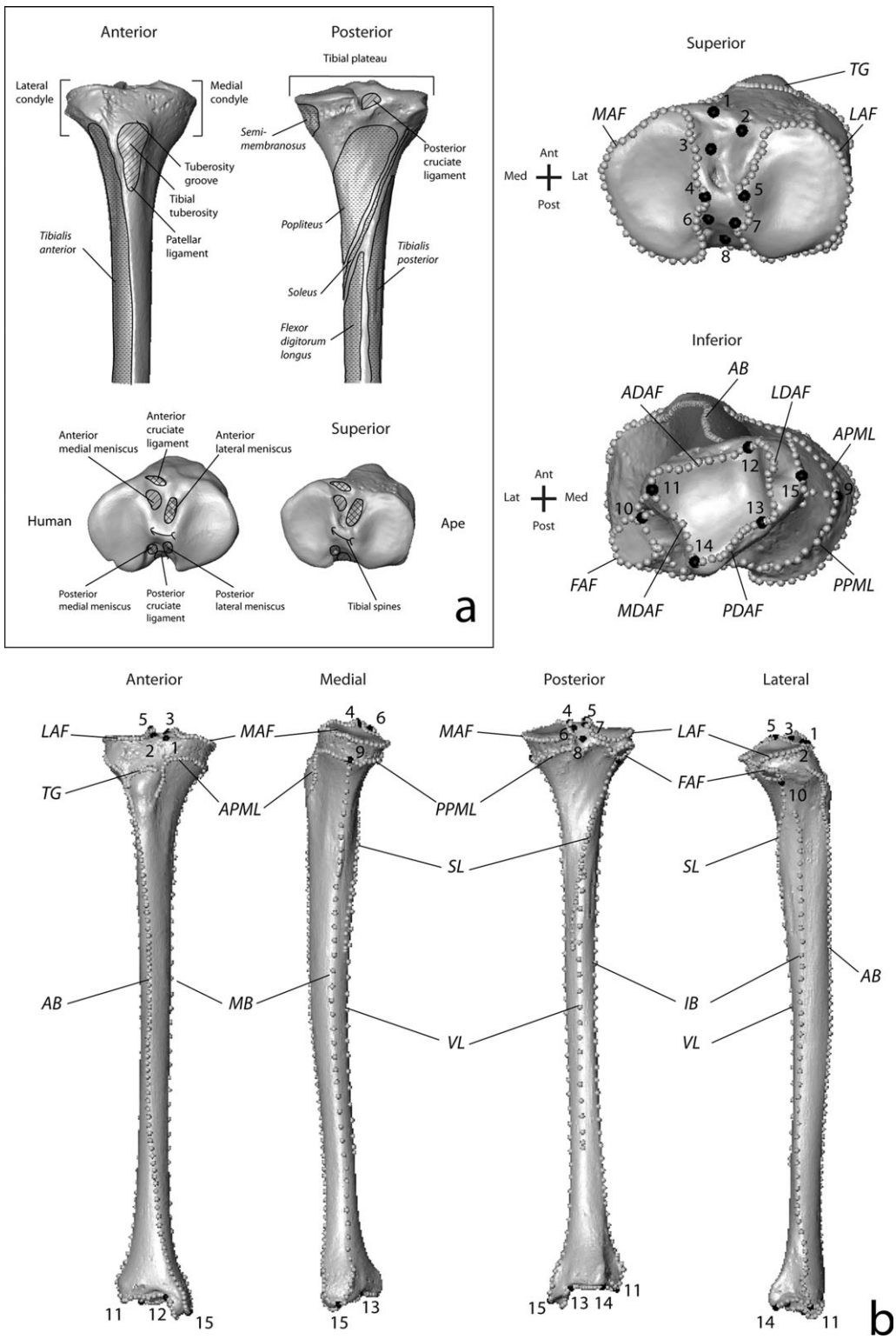

Fig. 1. (**a**) A human tibia labeled with the name of the anatomical regions used in the text, in anterior (upper left), posterior (upper right), and superior (lower left) views. The superior view of the tibial plateau in apes is also shown (lower right) to underline the difference in ligament attachments of the knee joint (after Senut and Tardieu, 1985). (**b**) A human tibia with our 498 landmarks and semilandmarks, in superior (upper right), inferior (middle right), anterior, medial, posterior, and lateral (lower, from left to right) view. In black are anatomical landmarks (15) and in gray are semilandmarks on curves (483). Names of the landmarks and curves are as listed in Tables 1 and 2, respectively.

TABLE 1. List of landmarks shown in Figure 1

Landmarks	Type	Label in Figure 1
Centroid of the anterior insertion of the medial meniscus	III	1
Most anterior point on the (anterior) attachment[a] of the lateral meniscus	II	2
Centroid of the insertion of the anterior cruciate ligament	III	3
Tip of the medial intercondylar eminence	II	4
Tip of the lateral intercondylar eminence	II	5
Centroid of the posterior insertion of the medial meniscus	III	6
Most posterior point on the (posterior) attachment[a] of the lateral meniscus	II	7
Centroid of the insertion of the posterior cruciate ligament	III	8
Most proximal point of the medial border on the metaphyseal line, beneath the groove on the medial condyle	II	9
Most proximal point on the soleal line, often faintly marked tubercle just inferior to the fibular facet	II	10
Most anterolateral point on the distal articular surface	II	11
Most anteromedial point on the distal articular surface	II	12
Most posteromedial point on the distal articular surface	II	13
Most posterolateral point on the distal articular surface	II	14
Tip of the malleolus	II	15

[a] The lateral meniscus has a unique attachment in apes while humans have an anterior and a posterior attachment. In this case, the most anterior point is taken on the anterior insertion and the most posterior point on the posterior one.

TABLE 2. List of curves and number of semilandmarks shown in Figure 1

Semilandmarks on curve	Type	Label in Figure 1	*N*
Lateral articular facet	Observed	LAF	49
Medial articular facet	Observed	MAF	49
Proximal fibular articular facet	Observed	FAF	20
Tuberosity groove	Ridge	TG	20
Anterior proximal metaphyseal line of the shaft	Observed	APML	24
Posterior proximal metaphyseal line of the shaft	Observed	PPML	24
Anterior border of the shaft	Ridge	AB	99
Interosseous border of the shaft	Ridge	IB	49
Medial border of the shaft	Ridge	MB	48
Soleal line	Ridge	SL	29
Vertical line	Ridge	VL	20
Anterior border of the distal articular facet	Observed	ADAF	13
Lateral border of the distal articular facet	Observed	LDAF	8
Posterior border of the distal articular facet	Observed	PDAF	13
Medial border of the distal articular facet	Observed	MDAF	18
Total No. semilandmarks			483

Apart from our preliminary reports (Frelat et al., 2008, 2009, 2010), we have found no other quantitative anthropometric analyses of the overall tibial surface. Rather, the typical investigation involves only a limited set of landmarks or focuses on a specific joint surface (Organ and Ward, 2006; Harcourt-Smith et al., 2008; Turley et al., 2011). To evaluate how features on the epiphyses and characteristics of the diaphysis covary, we introduce a method that captures and analyses in one single rigid structure the entire tibial external morphology using hundreds of measuring points. We can thus describe the relationships among size, shape and orientation of the articulations, positions of muscles, and shape of the shaft. After standard Procrustes analysis in shape and form space, we suggest reducing the dominating effect of variation in shaft length by computing affine-adjusted Procrustes shape coordinates in a novel way. Our purpose is to improve the visualization of effects of species and sex upon the form of the bones.

This article aims thus to provide a GM technique enriched by a novel and alternative version of that nonaffine projection, one that better matches the symmetries of the descriptions we apply to the form of the tibia (length versus cross-sections). The result of this nonstandard correction should be thought of as the intentional amplification of a certain residual signal in order to circumvent the effects of a known cause (species) on the unadjusted configuration [the original form of the bone, including the dominance of the length of the shaft in the standard formula for centroid size (CS)].

MATERIALS

We collected data from 77 tibiae of four extant hominoids: *Homo sapiens* (n = 28, 13 females, 11 males, and 4 indeterminate), *Gorilla gorilla* (n = 20, 7 females and 13 males), *Pan troglodytes* (n = 19, 12 females and 7 males), and *Pongo pygmaeus* (n = 10, 6 females and 4 males). Human tibiae are from the Pöch collection of Bushman remains (n = 20) of the Department of Anthropology, University of Vienna, Austria, and the Gars Thunau archeological collection (n = 8) of the Department of Anthropology, Natural History Museum of Vienna. Most of the Great Apes tibiae are from the Schultz Collection at the Institute and Museum of Anthropology, University of Zurich, Switzerland, while a few are housed in the Department of Zoology, Natural History Museum of Vienna. Only adult tibiae free of pathologies were included in this study.

METHODS

All morphometric and statistical analyses were performed in R (R Development Core Team, 2011) based on programs written by SK and MAF. Surface representations were produced in Amira 5.3.0 by MAF.

GM analysis

Each tibial surface was scanned with a triTOS surface scanner (Breuckmann Gmbh). We analyzed mostly right tibia; any left tibiae were mirrored first. All of them were aligned with the coordinate axes so that the main axis of the shaft corresponded to the z-axis and the maximum mediolateral length of the tibial plateau corresponded to the x-axis. The yz-plane corresponded then to the sagittal plane of the bone. For each 3D model of the whole tibia, a set of 15 landmarks (Table 1) and 483 semilandmarks on curves (Table 2) was digitized in the Rapidform 2006 software package by one of the authors (MAF). The 15 "real" landmarks lie on epiphyses (Fig. 1b). As there are no Type I landmarks (juxtaposition of tissues or equivalent;

Bookstein, 1991) on the tibia, our landmarks are variously of Type II (extremes of curvature characterizing single structures) or Type III (constructed points) such as centroids of ligament attachment areas. The latter were computed automatically in Rapidform from the border of the areas and projected onto the surface (see Table 1). To capture diaphyseal shape, semilandmarks were equidistantly digitized on observed curves such as the borders of epiphyseal articular surfaces and crest-lines created by muscular attachments on the diaphysis (Table 2 and Fig. 1a,b). We located enough semilandmarks to reproduce most of the individual measurements that others have used to characterize variations in this bone and to capture and sample the relatively large expanse of otherwise uncharted shaft surface. The complete set of semilandmarks was slid along curves to minimize the bending energy of the thin-plate spline (TPS) function (Bookstein, 1991). For further statistical analyses, those 483 relaxed semilandmarks (Fig. 1b) are treated as geometrically homologous points across all the specimens of the sample (Bookstein, 1997; Gunz et al., 2005).

In order to place an upper limit to the effect of intraobserver error in landmark digitization upon the ultimate analyses, we selected five tibiae for redigitizing the 15 landmarks three times at intervals of at least a week by one of us (MAF). We calculated mean-squared Procrustes distance of each replicated form from its mean (replication mean square error) and mean-squared Procrustes distance between all 77 cases, taken once each, and the grand mean (total mean square error). Then the intraobserver error is given by the ratio of replication mean square error to total mean square error. The mean of all five ratios was 0.00996. We were expecting this rather high value because none of our landmarks correspond to the Type I defined by Bookstein (1991).

The 77 configurations were transformed into shape coordinates by generalized Procrustes analysis (Rohlf and Slice, 1990). This procedure involves translating, rescaling, and rotating configurations relative to each other so as to minimize the overall sum of squared distances between corresponding (semi)landmarks. Rescaling usually adjusts landmark coordinates so that each configuration has a unit CS [square root of the summed squared Euclidean distances from all (semi)landmarks to their center of gravity; Bookstein 1991]. Procrustes shape coordinates were then subjected to principal component analysis (PCA) in both shape space and form space (Mitteroecker et al., 2004).

The artificial nonaffine component

To this point, our procedure has followed the standard Procrustes protocol. All landmarks are treated in precisely the same way and likewise all semilandmarks that have been slid on their curves. However, another symmetry of the Procrustes toolkit causes difficulties since Procrustes procedures treat all spatial directions of a geometry in the same way. Variations along the long axis of the tibia have been considered as of equal importance to variations within the planes of the articulations at the proximal and distal epiphyses. In the resulting superpositions, the variation of the shaft length dominates any other variation that may occur (Fig. 2b). This dominating effect is not due to the relative density of points along the shaft to points on the epiphyses—that will not affect any of the estimates of these axes—but rather to the structure and the length of the tibia itself. In this case, dividing by CS is almost exactly the same as dividing by maximal length of the tibia. We, therefore, scaled each tibia separately so that all three of the spatial axes (x, y, z) contribute in a fixed ratio of weights (Fig. 2c).

Variation of bone length with respect to its width, its depth, or their root mean square can be construed as one version of the affine component of shape variation (Rohlf and Bookstein, 2003), so what we have done can be interpreted as a novel, and thus artificial, alteration of this component. Any change in a configuration of landmarks or semilandmarks can be thought of as the sum of an affine component (Fig. 2a, upper right and lower left) and a nonaffine component (Fig. 2a, lower right). The affine component of a deformation is the portion of observed shape change that globally transforms the standard Cartesian coordinate system into a new grid where all stretching and compression are the same everywhere in space and in every direction. There are several ways of estimating the uniform part of any transformation (Bookstein, 1991), all of them sharing the usual symmetries of Procrustes distance as weighting all Euclidean directions equally. Our artificial affine transformation breaks that symmetry of the Procrustes distance formula and results in all three of the spatial axes (x, y, z) contributing with commensurate weights. For each form, z coordinates (longitudinal axis of the tibia) are scaled by the square root of the within-case z-coordinate variance and the x and y coordinates (AP and ML directions) by the square root of the sum of the within-case x- and y-coordinate variances. After this artificial affine scaling, variability along the longitudinal axis of the bone and variability perpendicular to this direction will contribute equally to the final shape distances. Compared to the original coordinates (Fig. 2b), influence of shaft length is no longer disproportionate but now is weighted equally with the net variability of the two other directions (Fig. 2c). Subsequently, all specimens are fitted again by means of a generalized Procrustes analysis, the resulting forms bringing the PCA out from under the strong dominance of the length of the bone.

Visualizations

To describe shape variations among hominoids, for each species, we constructed mean shapes of tibial surfaces both in the original space and in the affine-rescaled space. The tibial surface representations (target, T) corresponding to the deformation of the mean shape (consensus, C) along the PC axes were computed using the triangulated surface mean shapes and the TPS as an interpolation function (Bookstein, 1991). To ease visualization of shape deformations, TPS warps were extrapolated by factors k_i, where in shape space

$$T_i = C \pm k_i \times \text{eigenvector}[\text{shape}]_i$$

and in form space

$$T_i = (C \pm k_i \times \text{eigenvectors}[\text{shape}]_i) \times \exp(k_i \times \text{eigenvector}[\text{size}]_i),$$

where

$$k_i = 2 \times \text{sqrt}(\text{eigenvalue}_i)$$

to express two standard deviations, in order to scale standard deviations in the direction of the ith PC. (Eigenvectors are presumed to be unit vectors.)

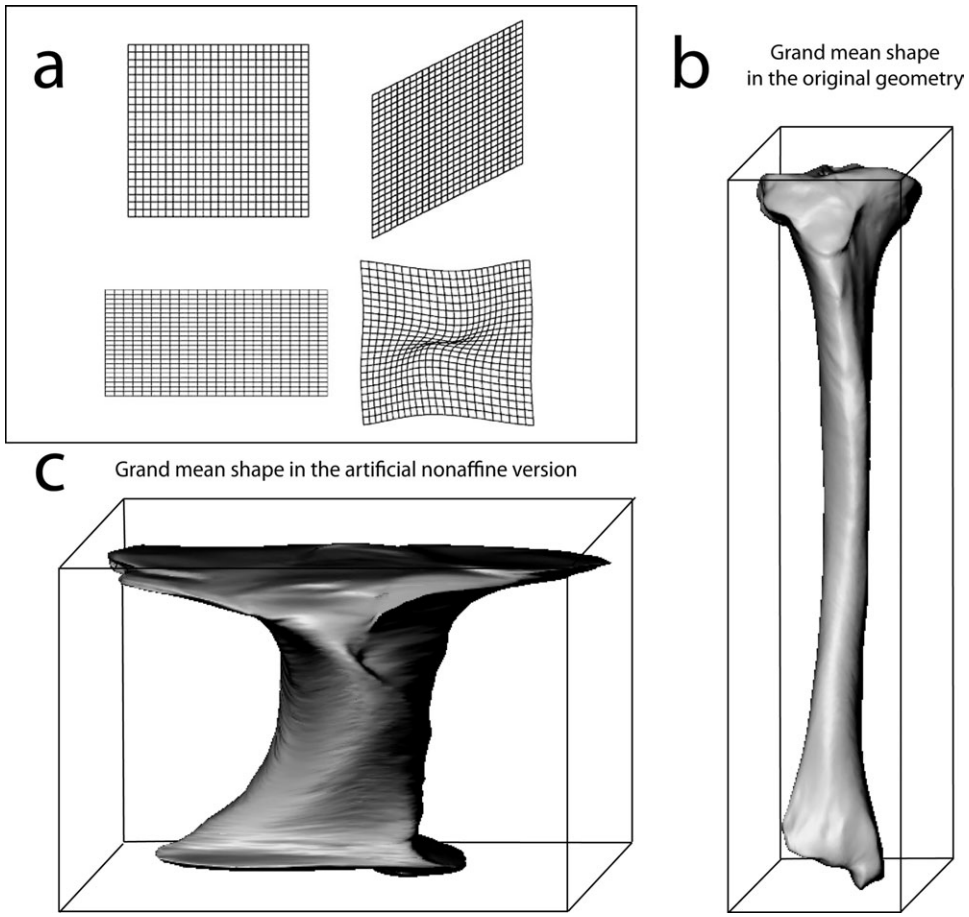

Fig. 2. (**a**) Transformations of a square grid (upper left): affine transformations (shear, upper right, and scaling in *x*-axis direction, lower left), involving simple stretching/compression in orthogonal directions that are the same everywhere in the space; and nonaffine transformation (lower right), carrying local "bending" involving twisting, stretching, and shifting of small regions (from Slice, 2005). Comparison of the grand mean shape in the original geometry of the surface scans (**b**) with the artificial nonaffine version of it (**c**).

RESULTS AND DISCUSSION

Shape space PCA (before affine adjustment)

The first PC explains approximately 40% of total shape variation and the second PC almost 16% (Fig. 3). The main deformations on PC1, as illustrated by the first row of tibial surface representations (Fig. 3), generally correspond to the locomotor-related differences between apes and humans known from the literature (e.g., Martin and Saller, 1959; Trinkaus, 1975; Lewis, 1981; Stern and Susman, 1983; Tardieu, 1981, 1988; Senut and Tardieu, 1985; Susman et al., 1984; Latimer et al., 1987; Aiello and Dean, 2002), such as size of the medial condyle, shape of the tuberosity, pattern of muscle attachments on the shaft, curvature of the shaft, or position of the insertions of the menisci and of the cruciate ligaments (Fig. 1a). Thus, variation on PC1 clearly separates bipeds from nonbipeds. African apes are not separated from Asian apes, but the two human groups seem to spread out differently, the Austrian group clustering in the higher range of the human variation.

On PC2, *Gorilla* and *Pan* form distinct clusters with minor overlap, and the medieval Austrian specimens clearly separate from the Bushmen. *Pongo* overlap with both African species: male *Pongo* cluster with *Gorilla* and female *Pongo* with *Pan*. Variation on PC2 is less complicated (Fig. 3, second row of tibial surface representations) and generally relates to overall tibial robusticity (diaphyseal thickness in relation to bone length; Martin and Saller, 1959)—especially in the ML dimensions, the posterior projection of the tibial plateau, the degree of torsion of the distal epiphysis relative to the tibial plateau, and the size and orientation of the distal epiphysis. Compared to *Pan* and female *Pongo* on one side and the Bushmen on the other, *Gorilla* and male *Pongo* and the Austrian group have a thicker shaft and relatively bigger epiphyses, respectively. Their shaft also shows less torsion, condyle articular facets are more balanced, and their tibiotalar plane shows a slight angulation relative to the horizontal. Those morphological features are coupled with a shortened and laterally displaced vertical line and an elongated soleal line, implying a greater posterior area for the flexor digitorum longus (plantarflexion of the ankle and foot) on the posterior face, a displacement of the tibialis posterior (plantarflexion, inversion) on the lateral face at the expense of the tibialis anterior (dorsiflexion, inversion). Those variations are consistent with differences in locomotor behavior among apes, both *Pan* and *Gorilla* being knuckle-walkers with different degree of arboreal activity, but at very different body sizes (Reynolds, 1987; Larson et al., 2001; Polk et al., 2009). However, this analysis

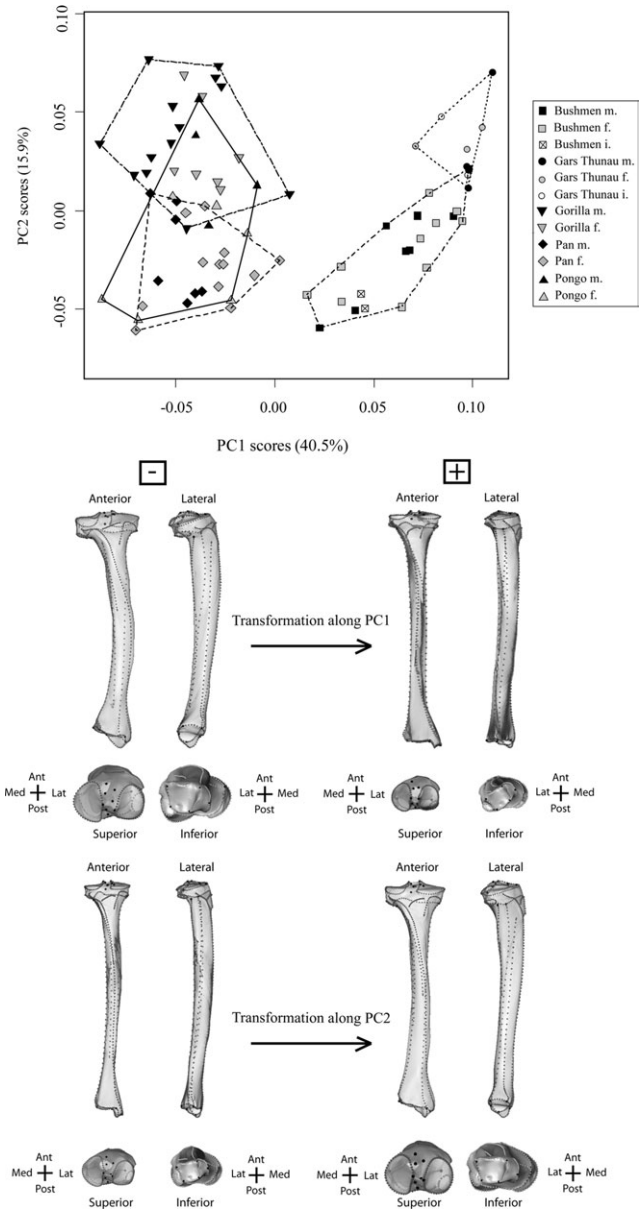

Fig. 3. PC scores of the Procrustes shape coordinates in shape space. The four groups of tibial surface representations, visualized in anterior, lateral, superior, and inferior view, are extreme deformations of the average shape along PC1 and PC2. To ease visualization of shape differences, deformations are extrapolated.

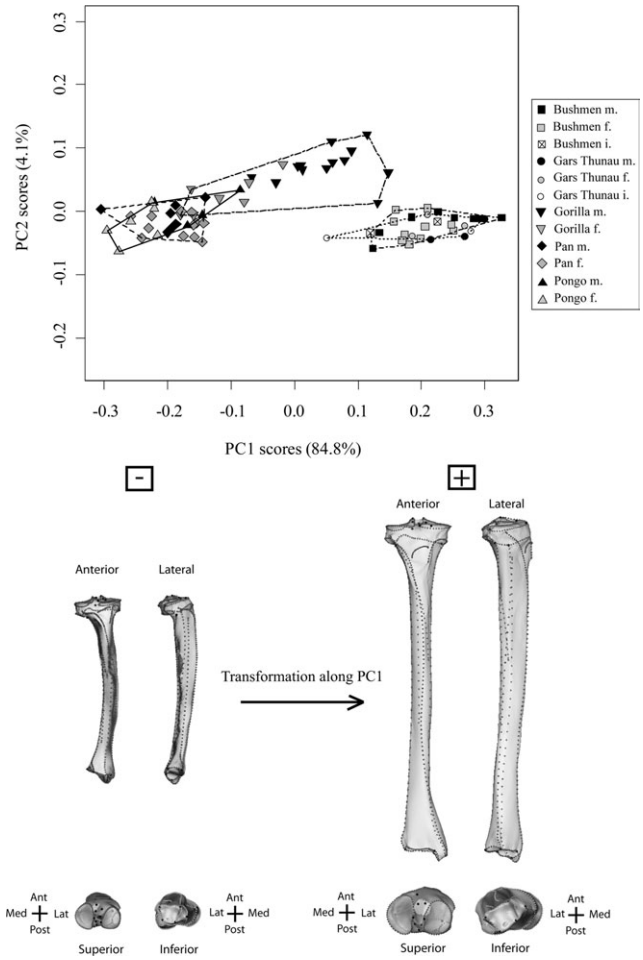

Fig. 4. PC scores of the Procrustes shape coordinates in form space. The four groups of tibial surface representations, visualized in anterior, lateral, superior, and inferior view, are extreme deformations of the average shape along PC1.

fails to highlight clear shape differences between *Pongo* and the African apes. On the contrary, *Pongo* overlap with both species, males clustering with *Gorilla* and females with *Pan*. Yet within-species allometry is not detected, eliminating the effect of body size as a plausible explanation. Better hypotheses for those differences may lie in their different behaviors, which are probably the consequence of substrate-use constraints imposed on large-bodied gorillas and male orangutans (Cant, 1992; Hunt, 1992; Remis, 1995; Doran, 1996; Gebo, 1996; Carlson, 2005; Thorpe and Crompton, 2006). These results are consistent with other studies that focused on femoral articular morphology and/or femoral shaft strength (Tardieu, 1983; Ruff, 2002; Harmon, 2007) but show some slight differences with what has been described by a recent GM study using a limited number of landmarks (see below, Turley et al., 2011). However, more human specimens, with known main activities, are needed to be able to interpret human shape variation.

Form space PCA (before affine adjustment)

When CS is reintroduced into the data set (form space, Fig. 4), PC1 (84.8% of the total Procrustes form variance) expresses overall size increase and static within-species allometry while PC2 explains only about 4% of the variation. As CS is highly influenced by overall tibial length, variation along PC1 depicts a significant elongation of the tibial shaft coupled with an increase in the dimensions of the epiphyses. Those size changes are associated with the typical morphological differences between the species as already described in shape space PC1 (see above and Fig. 3, first row). Shape deformations along form space PC2 are not shown here as they are predominantly the same as those visualized in shape space (Fig. 3, second row) and generally involve increase of overall tibial robusticity.

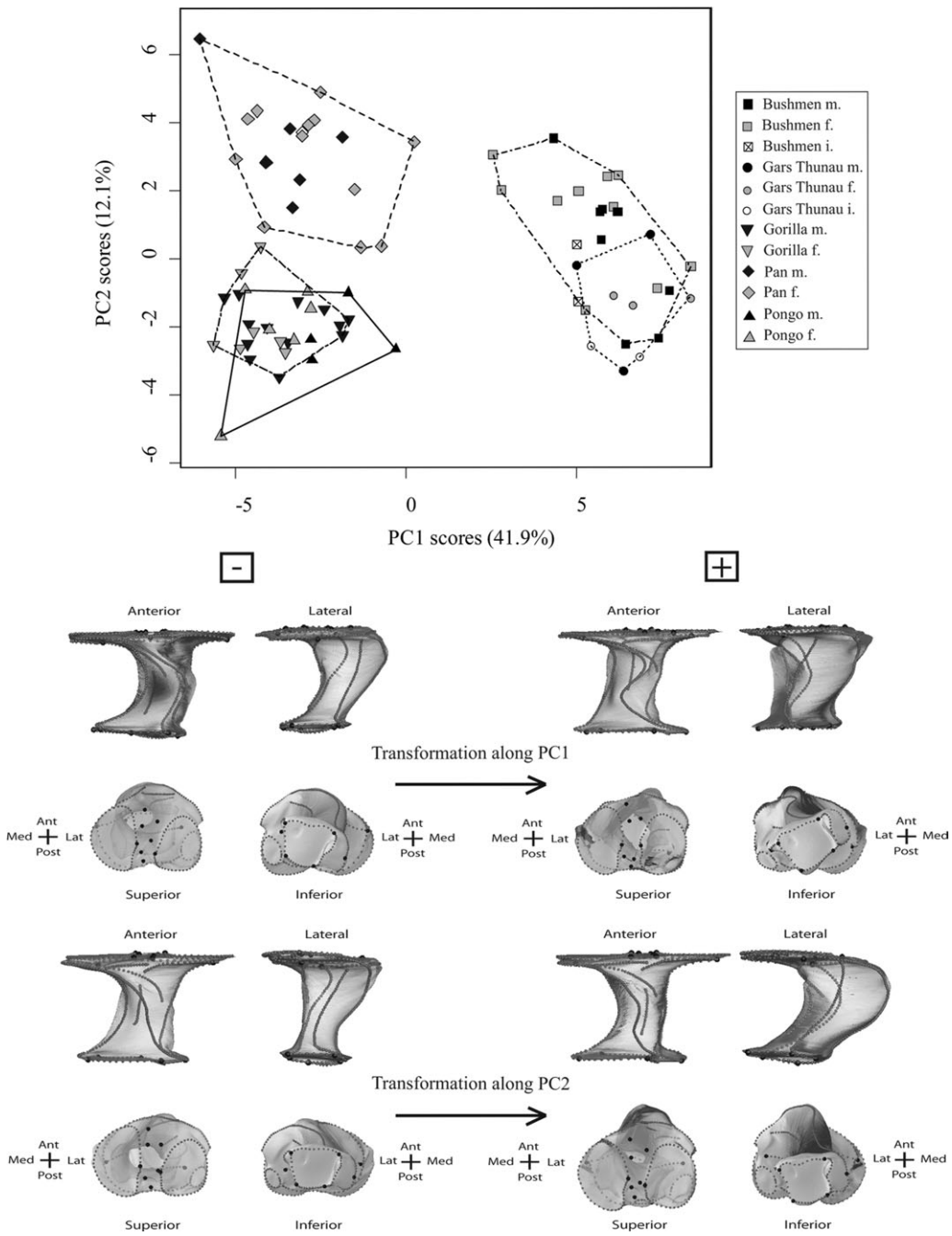

Fig. 5. PC scores of the scaled (nonaffine component) Procrustes shape coordinates in shape space. The four groups of tibial surface representations, visualized in anterior, lateral, superior, and inferior view, are extreme deformations of the average shape along PC1 and PC2.

Human and ape allometric trajectories are clearly distinct, even parallel, suggesting that CS or tibial length influences human and ape tibiae similarly. While apes and modern human have different mean shapes, the trajectories describe similar shape transformations. Shorter tibiae of both human and non-human sample exhibit a more curved shaft and relatively broad epiphyses while longer tibiae are straight and have relatively narrow epiphyses (see discussion below). Our results regarding human and non-human static allometry are consistent with previous investigations of diverse anatomical regions using either GM or more traditional methods (e.g., Jungers, 1982; Jungers and Stern, 1983; Ackerman and Krovitz, 2002; Kidd and Oxnard, 2002; Penin et al., 2002; Mitteroecker et al., 2004). They support earlier descriptions referring to morphological relationship between *Gorilla* and *Pan* as evidence of a "peramorphic" pattern of morphology produced by hypermorphosis (the extension of common growth patterns to larger sizes: Gould, 1975; Shea, 1983).

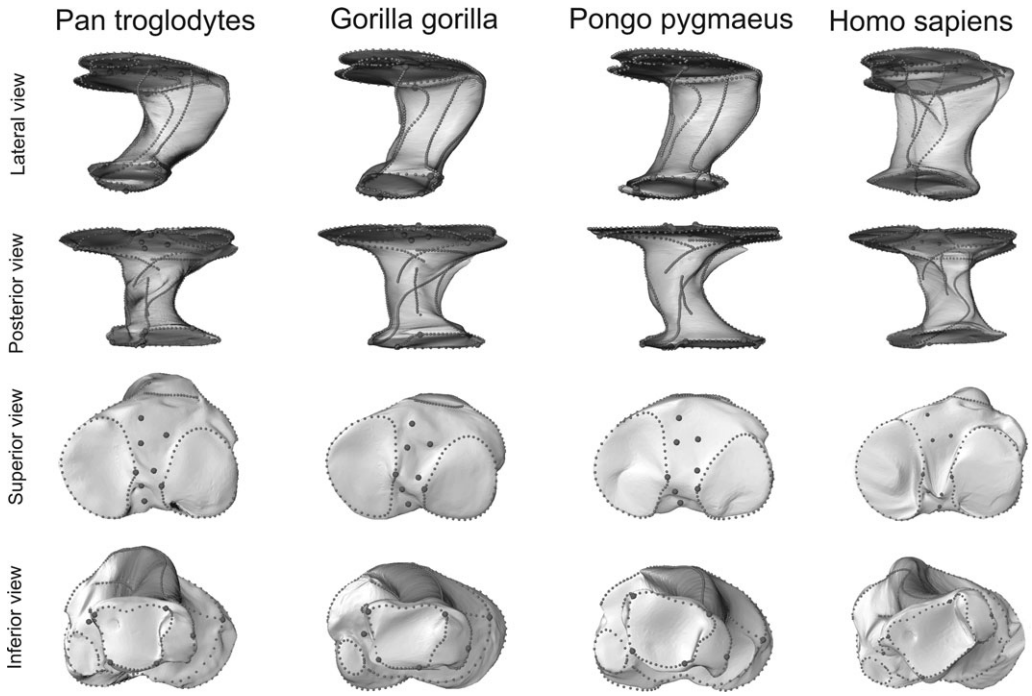

Fig. 6. Differences between the tibial mean shape of the four species of hominoids visualized in the scaled space, after the artificial affine transformation (from left to right: *P. troglodytes*, *G. gorilla*, *P. pygmaeus*, and *H. sapiens*). Top row: lateral view; second row: posterior view; third row: superior view; bottom row: inferior view.

PCA of our "artificial nonaffine component"

After we altered the affine component of the data as described above, the eigenvalues of PC1 and PC2 show only little change (variation on PC1 is now 42%, and 12% on PC2) but our species cluster rather more neatly (Fig. 5). Again, variation on PC1 depicts the typical morphological differences between the species observed in shape and form space (Fig. 5, first row).

On PC2, however, the artificial affine transformation results in a rather different grouping of the non-human species than the unscaled analysis did (Fig. 3). *Pan* cluster well away from *Gorilla* and *Pongo*, which clearly overlap one another. Deformations along PC2 are mainly due to the anteroposteriorly more curved diaphysis, associated with a wider attachment area for the tibialis posterior and a longer one for the flexor digitorum tibialis, both of which provide stability to the ankle joint. *Pan* tibiae are more anteroposteriorly curved and, also, show more axial torsion than those of *Gorilla* and *Pongo* (Fig. 6). These features are associated with the posterior displacement of the distal epiphysis. *Pan* also has more balanced condyle areas, a proximal facet for the fibula that expands anteriorly and medially, and a squarer distal trochlear surface. It seems that the same trend exists in humans, where a large fraction of Bushmen (hunter-gatherers) has an anteriorly curved tibia while Austrian individuals (agriculturalists) have straighter tibiae and cluster near the bottom of the Bushman range. But, here again more human specimens are needed to be able to interpret human shape variation. The biomechanical role and the adaptive meaning of limb bone curvature, the main feature responsible for the variation on PC2, is not quite straightforward (Bertram and Biewener, 1988; Shackleford and Trinkaus, 2002; Yamanaka et al., 2005; De Groote et al., 2010). As summarized by De Groote et al. (2010), "curvature in combination with muscle and joint reaction forces may 1) lower bending stress by translating bending stress to axial compression, 2) facilitate muscle expansion and packing, 3) be a compromise between bone strength and predictability of bending strains and material feature, or 4) bring the muscle mass closer to the overall longitudinal axis of the diaphysis." Since the areas of insertions of two of the muscles providing stability of the ankle are largest in *Pan*, their higher curvature could be related to the relative size or position of those muscles. It could also be related to differences in mechanical loading, i.e., bending, due to substrate preferences or various components of locomotor behavior. Those results are consistent with the fact that Turley et al. (2011) did not find the presumed similarities between *Gorilla* and *Pan*, especially regarding tibial articular morphology. Our analysis thus seems to accord with their hypothesis that those two species differ in their mode of locomotion, although this might not be related to size since we did not find any correlation with CS.

Finally, on PC3, *Gorilla* and *Pongo* separate (5% of the scaled shape variation) with minor overlap (figure not shown here). This variation is mainly due to axial torsion and anteroposterior curvature of the shaft and relative size of the epiphyses (Fig. 6). *Pongo* have greater axial rotation and curvature of the shaft and broader articular surfaces, consistent with arboreal activity and terrestrial fist-walking (Fig. 6). On the other side, *Gorilla* exhibits a more trapezoidal tibiotalar surface associated with an anterior displacement of the medial malleolus (Fig. 6), consistent with what the increase in mass entails for stabilizing up terrestrial activity or vertical climbing (DeSilva, 2009). Those results are consistent with the findings by Turley et al. (2011) and previous observations among extant hominoids (Latimer et al., 1987; Turley et al., 2008).

CONCLUSIONS

The present study demonstrates that GM is an effective tool for investigating tibial shape in 3D and introduces a new method, an artificial affine transformation, to eliminate the dominating effect of the long shaft when comparing humans and non-humans. Among the advantages of our method, we note that most features hitherto described in the literature that distinguish modern humans from apes can be captured and visualized as well by an approach based on landmarks and semilandmarks (Fig. 1b). But, beyond that, it allows investigators to visualize the covariation of the three functionally distinct parts of the tibia that are the two epiphyses and the diaphysis (Figs. 3–5) and to separate size from shape in the analysis (compare Figs. 3 and 4). For example, compared to the above-mentioned GM studies of long bones, our method is able to highlight the relationship between shaft curvature, muscle position, relative size and shape of the condyles, and shape and orientation of the tibiotalar articular surface (Figs. 3–6). Altogether, our study of the tibia demonstrates that a comprehensive GM approach can be applied to hominoid long bone elements. It can be used to study shape or form separately, and it can scale the influence of the dominating shaft.

Compared with traditional osteometry, another advantage of the introduction of the artificial affine component is that it not only confirms the differentiation between bipeds and nonbipeds (Figs. 3–5) but also distinguishes tibial shapes both among non-human hominoids (Figs. 5 and 6) and among humans (Figs. 3 and 5). Those shape variations may be related to different locomotor and positional behavior, to substrate preferences among nonbipedal Great Apes (e.g., Reynolds, 1987; Cant, 1992; Hunt, 1992; Remis, 1995; Doran, 1996; Larson et al., 2001; Carlson, 2005; Thorpe and Crompton, 2006; Polk et al., 2009), or to distinct activity patterns in human populations (Ruff et al., 1984; Ruff, 1987; Bridges, 1995; Carlson et al., 2007; Stock and Shaw, 2007; Shaw and Stock, 2009, 2011; Shaw and Ryan, 2011). Further investigation may reveal how the morphological variation quantified in this study is related to locomotion/activity patterns, phylogeny, and development, a topic beyond the scope of this article.

Of course, the new method has some drawbacks as well. Scaling the tibia flattens its geometry at the epiphysis, putting all 3D variation in this region into what would appear to be a single plane. Shape changes on the epiphyses are no longer correctly rendered. Those features must be examined in the original shape space instead (Figs. 3 and 4).

While locomotor information may be inferred from our results to some extent, only a combination of GM with biomechanical approaches will permit a thorough understanding of how external shape and form are associated to bone structural strength.

ACKNOWLEDGMENTS

We thank Christine Tardieu, Bence Viola, Philipp Mitteroecker, Kristian Carlson, Michael Coquerelle, Colin Shaw, and Caroline Simonis for helpful discussions and support in the course of this study. We are also grateful to Maria Teschler-Nicola, Barbara Herzig, Christopher Zollikofer, and their staff for allowing access to the specimens in their care. Special thanks go to Alexandre Bourdeu for his assistance with the Breuckmann Scanner in the Department of Anthropology of the University of Vienna. The authors are grateful for the comments of the Associate Editor and two anonymous reviewers on an earlier draft.

LITERATURE CITED

Ackermann RR, Krovitz GE. 2002. Common patterns of facial ontogeny in the hominid lineage. Anat Rec 269:142–147.

Aiello L, Dean C. 2002. An introduction to human evolutionary anatomy. San Diego: Elsevier Academic Press.

Bastir M, Rosas A. 2006. Correlated variation between the lateral basicranium and the face: A geometric morphometric study in different human groups. Arch Oral Biol 51:814–824.

Berger LR, Tobias PV. 1996. A chimpanzee-like tibia from Sterkfontein, South Africa and its implications for the interpretation of bipedalism in *Australopithecus africanus*. J Hum Evol 30:343–348.

Bertram JE, Biewener AA. 1988. Bone curvature: sacrificing strength for load predictability? J Theor Biol 131:75–92.

Bookstein FL. 1991. Morphometric tools for landmark data: geometry and biology. Cambridge: Cambridge University Press.

Bookstein FL. 1997. Landmark methods for forms without landmarks: morphometrics of group differences in outline shape. Med Image Analysis 1:225–243.

Bookstein FL, Schaefer K, Prossinger H, Seidler H, Fieder M, Stringer C, Weber G, Arsuaga J, Slice D, Rohlf F, Recheis W, Mariam A, Marcus L. 1999. Comparing frontal cranial profiles in archaic and modern *Homo* by morphometric analysis. Anat Rec 257:217–224.

Bouhallier J, Berge C, Penin X. 2004. Procrustes analysis of the pelvic cavity in australopithecines (AL 288, STS 14), humans and chimpanzees: obstetrical consequences. Comptes Rendu Palevol 3:295–304.

Bridges PS. 1995. Skeletal biology and behavior in ancient humans. Evol Anthropol 4:112–120.

Cant JGH. 1992. Positional behavior and body size of arboreal primates: a theoretical framework for field studies and an illustration of its application. Am J Phys Anthropol 88:273–283.

Carlson KJ. 2005. Investigating the form-function interface in African apes: relationships between principal moments of area and positional behaviors in femoral and humeral diaphyses. Am J Phys Anthropol 127:312–334.

Carlson KJ, Grine FE, Pearson OM. 2007. Robusticity and sexual dimorphism in the postcranium of modern hunter-gatherers from Australia. Am J Phys Anthropol 134:9–23.

Coquerelle M, Bookstein FL, Braga J, Halazonetis DJ, Weber GW, Mitteroecker P. 2011. Sexual dimorphism of the human mandible and its association with dental development. Am J Phys Anthropol 145:192–202.

De Groote I. 2011. Femoral curvature in Neanderthals and modern humans: a 3D geometric morphometric analysis. J Hum Evol 60:540–548.

De Groote I, Lockwood CA, Aiello L. 2010. Technical note: a new method for measuring long bone curvature using 3D landmarks and semi-landmarks. Am J Phys Anthropol 141:658–664.

DeSilva JM. 2009. Functional morphology of the ankle and the likelihood of climbing in early hominins. Proc Natl Acad Sci USA 106:6567–6572.

Doran DM. 1996. The comparative positional behavior of the African apes. In: McGrew W, Nishida T, editors. Great Ape societies. Cambridge: Cambridge University Press. p 213–224.

Frelat MA, Bookstein FL, Weber GW. 2008. Variation of human tibial shape: a 3D approach using virtual specimens [abstract]. Bull Mém Soc Anthropol Paris 20:38.

Frelat MA, Bookstein FL, Weber GW. 2009. Tibial shape analysis—a quantitative approach for the whole bone [abstract]. Am J Phys Anthropol Suppl 48:130.

Frelat MA, Katina S, Weber GW, Bookstein FL. 2010. An affine-adjusted analysis of tibial shape in hominoids [abstract]. Am J Phys Anthropol Suppl 50:93–94.

Gebo DL. 1996. Climbing, brachiation, and terrestrial quadrupedalism: historical precursors of hominid bipedalism. Am J Phys Anthropol 101:55–92.

Gould SJ. 1975. Allometry in primates, with emphasis on scaling and the evolution of the brain. In: Szalay F, editor. Approaches to primate paleobiology. Basel: Karger Contr Primatol. p 5244–5292.

Gunz P, Mitteroecker P, Bookstein FL. 2005. Semilandmarks in three dimensions. In: Slice DE, editor. Modern morphometrics in physical anthropology. New York: Kluwer Academic. p 73–98.

Harcourt-Smith WEH, Tallman M, Frost SR, Wiley DF, Rohlf FJ, Delson E. 2008. Analysis of selected hominoid joint surfaces using laser scanning and geometric morphometrics: a preliminary report. In: Sargis EJ, Dagosto M, editors. Mammalian evolutionary morphology: a tribute to Frederick S. Szalay. Dordrecht: Springer Science + Business Media BV. p 373–383.

Harmon EH. 2006. Size and shape variation in *Australopithecus afarensis* proximal femora. J Hum Evol 51:217–227.

Harmon EH. 2007. The shape of the hominoid proximal femur: a geometric morphometric analysis. J Anat 210:170–185.

Harmon EH. 2009a. The shape of the early hominin proximal femur. Am J Phys Anthropol 139:154–171.

Harmon EH. 2009b. Size and shape variation in the proximal femur of *Australopithecus africanus*. J Hum Evol 56:551–559.

Havarti K. 2003. Quantitative analysis of Neanderthal temporal bone morphology using three-dimensional geometric morphometrics. Am J Phys Anthropol 120:323–338.

Hunt KD. 1992. Positional behavior of *Pan troglodytes* in the Mahale Mountains and Gombe Stream National Parks, Tanzania. Am J Phys Anthropol 87:83–105.

Jungers WL. 1982. Lucy's limbs: skeletal allometry and locomotion in *Australopithecus afarensis*. Nature 297:676–678.

Jungers WL. 1987. Body size and morphometric affinities of the appendicular skeleton in *Oreopithecus bambolii* (IGF 11778). J Hum Evol 16:445–456.

Jungers WL, Harcourt-Smith WEH, Wunderlich RE, Tocheri MW, Larson SG, Sutikna T, Due RA, Morwood MJ. 2009. The foot of *Homo floresiensis*. Nature 459:81–84.

Jungers WL, Stern JT. 1983. Body proportions, skeletal allometry and locomotion in the Hadar hominids: a reply to Wolpoff. J Hum Evol 12:673–684.

Kidd RS, Oxnard CE. 2002. Patterns of morphological discrimination in selected human tarsal elements. Am J Phys Anthropol 117:169–181.

Larson SG, Schmitt D, Lemelin P, Hamrick M. 2001. Limb excursion during quadrupedal walking: how do primates compare to other mammals? J Zool Lond 255:353–365.

Latimer B, Ohman JC, Lovejoy CO. 1987. Talocrural joint in African hominoids: implications for *Australopithecus afarensis*. Am J Phys Anthropol 74:155–175.

Lewis OJ. 1989. Functional morphology of the evolving hand and foot. Oxford: Oxford University Press.

Lovejoy CO, Suwa G, Simpson SW, Matternes J, White TD. 2009. The great divides: *Ardipithecus ramidus* reveals the postcrania of our last common ancestors with African apes. Science 326:100–106.

Mahfouz M, Merkl B, Abdel Fatah EE, Booth R Jr, Argenson JN. 2007. Automatic methods for characterization of sexual dimorphism of adult femora: distal femur. Comput Methods Biomech Biomed Eng 10:447–456.

Marchi D. 2007. Relative strength of the tibia and fibula and locomotor behavior in hominoids. J Hum Evol 53:647–655.

Martin R, Saller K. 1959. Lehrbuch der Anthropologie in systematischer Darstellung, Vol. 2. Stuttgart: Gustav Fischer Verlag.

Mitteroecker P, Gunz P, Bernhard M, Schaefer K, Bookstein FL. 2004. Comparison of cranial ontogenetic trajectories among Great Apes and humans. J Hum Evol 46:679–697.

O'Higgins P. 2000. The study of morphological variation in the hominid fossil record: biology, landmarks and geometry. J Anat 197:103–120.

Organ JM, Ward CV. 2006. Contours of the hominoid lateral tibial condyle with implications for *Australopithecus*. J Hum Evol 51:113–127.

Penin X, Berge C, Baylac M. 2002. Ontogenetic study of the skull in modern humans and the common chimpanzees: neotenic hypothesis reconsidered with a tridimensional Procrustes analysis. Am J Phys Anthropol 118:50–62.

Polk JD, Williams SA, Peterson JV. 2009. Body size and joint posture in primates. Am J Phys Anthropol 140:359–367.

R Development Core Team. 2011. R: a language and environment for statistical computing. Vienna: R Foundation for Statistical Computing. http://www.r-project.org.

Remis M. 1995. Effects of body size and social context on the arboreal activities of lowland gorillas in the Central African Republic. Am J Phys Anthropol 97:413–433.

Reynolds TR. 1987. Stride length and its determinants in humans, early hominids, primates, and mammals. Am J Phys Anthropol 72:101–115.

Rohlf FJ, Bookstein FL. 2003. Computing the uniform component of shape variation. Syst Biol 52:66–69.

Rohlf FJ, Slice DE. 1990. Extensions of the Procrustes method for the optimal superimposition of landmarks. Syst Zool 39:40–59.

Ruff C. 1987. Sexual dimorphism in human lower limb bone structure: relationship to subsistence strategy and sexual division of labor. J Hum Evol 16:391–416.

Ruff CB. 2002. Long bone articular and diaphyseal structure in Old World monkeys and apes I: locomotor effects. Am J Phys Anthropol 119:305–342.

Ruff CB, Larsen CS, Hayes WC. 1984. Structural changes in the femur with the transition to agriculture on the Georgia coast. Am J Phys Anthropol 64:125–136.

Senut B, Tardieu C. 1985. Functional aspects of Plio-Pleistocene limb bones: implications for taxonomy and phylogeny. In: Delson E, Liss AR, editors. Ancestors: the hard evidence. New York: John Wiley & Sons. p 193–201.

Shackelford LL, Trinkaus E. 2002. Late Pleistocene human femoral diaphyseal curvature. Am J Phys Anthropol 118:359–370.

Shaw CN, Ryan TM. 2012. Does skeletal anatomy reflect adaptation to locomotor patterns? Cortical and trabecular architecture in human and nonhuman anthropoids. Am J Phys Anthropol 147:187–200.

Shaw C, Stock J. 2009. Intensity, repetitiveness, and directionality of habitual adolescent mobility patterns influence the tibial diaphysis morphology of athletes. Am J Phys Anthropol 140:149–159.

Shaw CN, Stock JT. 2011. The influence of body proportions on femoral and tibial midshaft shape in hunter-gatherers. Am J Phys Anthropol 144:22–29.

Shea BT. 1983. Allometry and heterochrony in the African apes. Am J Phys Anthropol 62:275–289.

Slice DE. 2005. Modern morphometrics in physical anthropology. New York: Kluwer Press.

Stern JT. 2000. Climbing to the top: a personal memoir of *Australopithecus afarensis*. Evol Anthropol 9:113–133.

Stern JT, Susman RL. 1983. The locomotor anatomy of *Australopithecus afarensis*. Am J Phys Anthropol 60:279–317.

Stock JT, Shaw C. 2007. Which measures of diaphyseal robusticity are robust? A comparison of external methods of quantifying the strength of long bone diaphyses to cross-sectional geometric properties. Am J Phys Anthropol 134:412–423.

Stringer C, Trinkaus E, Roberts M, Parfitt S, Macphail R. 1998. The Middle Pleistocene human tibia from Boxgrove. J Hum Evol 34:509–547.

Susman RL, Stern JT, Jungers WL. 1984. Arboreality and bipedality in the Hadar hominids. Folia Primatol 43:113–156.

Tardieu C. 1981. Morpho-functional analysis of the articular surfaces of the knee-joint in Primates. In: Chiarelli A, Corruccini R, editors. Primate evolutionary biology. Berlin: Springer-Verlag. p 68–80.

Tardieu C. 1983. L'articulation du genou: analyse morpho-fonctionnelle chez les primates et les hominidés fossiles. Paris: CNRS Editions.

Tardieu C. 1988. Evolution of the knee interarticular menisci in Primates and in some fossil hominids. In: Else JG, Lee PC, editors. Primate evolution. Cambridge: University Press. p 183–190.

Taylor AB, Slice DE. 2005. A geometric morphometric assessment of the relationship between scapular variation and locomotion in African apes. In: Slice DE, editor. Modern morphometrics in physical anthropology. New York: Kluwer Academic. p 299–318.

Thorpe SKS, Crompton RH. 2006. Orangutan positional behavior and the nature of arboreal locomotion in Hominoidea. Am J Phys Anthropol 131:384–401.

Trinkaus E. 1975. The Neandertals from Krapina northern Yugoslavia: an inventory of the lower limb remains. Z Morphol Anthropol 67:44–59.

Turley K, Guthrie EH, Frost SR. 2011. Geometric morphometric analysis of tibial shape and presentation among catarrhine taxa. Anat Rec 294:217–230.

Turley K, Henderson E, Frost S. 2008. Distal tibial shape and presentation reflect the type of substrate. Am J Phys Anthropol 135:210.

Vidarsdottir US, O'Higgins P, Stringer C. 2002. A geometric morphometric study of regional differences in the ontogeny of the modern human facial skeleton. J Anat 201:211–229.

Weber GW, Gunz P, Mitteroecker P, Stadlmayr A, Bookstein FL, Seidler H. 2006. External geometry of Mladec neurocrania compared with anatomically modern humans and Neandertals. In: Teschler-Nicola M, editor. Early modern humans at the Moravian gate. Vienna; New York: Springer-Verlag. p 453–471.

Yamanaka A, Gunji H, Ishida H. 2005. Curvature length and cross-sectional geometry of the femur and humerus in anthropoid primates. Am J Phys Anthropol 127:46–57.

Zipfel B, DeSilva JM, Kidd RS, Carlson KJ, Churchill SE, Berger LR. 2011. The foot and ankle of *Australopithecus sediba*. Science 333:1417–1420.